Supporting information

Stretchable Sensors with Tunability and Single Stimuli-Responsiveness through Resistivity Switching Under Compressive Stress

Jarkko Tolvanen[1], Joni Kilpijärvi[1], Olli Pitkänen[1], Jari Hannu[1], Heli Jantunen[1]*

[1] Microelectronics Research Unit, Faculty of Information Technology and Electrical Engineering, University of Oulu, P.O. Box 4500, FIN-90014 University of Oulu, Finland

*Corresponding author

E-mail: jarkko.tolvanen@oulu.fi

1. Supplementary Texts

1.1 Synthesis of composite and stencil printing process

A solution of urethane rubber with 5 wt % pyrolyzed pine content was mixed in a container and vacuum degassed. Then the solution was poured into polyimide taped silver-plated nylon (SPN) attached to a non-stick surface. After pouring, a biochar composite (BC) film layer was stencil printed onto the SPN and the structure was cured at room temperature. Then the second BC solution was prepared in a similar manner and stencil printed onto the first BC layer. When curing for the second time, a pressure was applied to the surface of the multilayered structure to control the penetration depth of the second BC layer into top SPN. The dimensions of the devices in terms of their thickness, length, and width were ~0.95-1.75 mm, ~23-26 mm and ~0.7-0.8 mm, respectively.

1.2 Layer-to-layer bonding improvement

The structure A with properly embedded BC/SPN interfaces can be elongated by ~250% before the sample slips from the clamps (force ~15 N). The structure A stays fully intact after testing. The structure B with improperly embedded BC/SPN interface leads to peeling of the SPN from to the BC film at 70% elongation (force ~7.5 N). The structure B is almost completely delaminated after stretching it over 200%.

1.3 Capacitive response under tensile strain

Capacitive response of the device under tensile strain can be expressed as Equation (S1):

$$\frac{\Delta C}{C_0} = \left(\left(\frac{\varepsilon_0 \varepsilon_r (1+\varepsilon) l_0 (1-v_{elec}\varepsilon) w_0}{(1-v_{diel}\varepsilon) d_0} + C_F\right) - C_0\right)/C_0 \qquad \text{(S1)}$$

where ε_0 is the relative permittivity of vacuum, ε_r is the relative permittivity of dielectric layer, ε is applied tensile strain, l_0 is initial length of the sensor, v_{elec} is the Poisson's ratio of electrodes, w_0 is the initial width of the sensor, v_{diel} is the Poisson's ratio of the dielectric layer and d_0 is the initial

thickness of the sensor. [1–3] The C_F is an error correction term for the fringing electric field effect around the electrode edges due to non-ideality of the parallel-capacitor's structural dimensions (i.e. ratio of electrode area to thickness).[2–3] This error correction term is negligible for BC/SPN. As known, typical Poisson's ratios for polymers are in the range of 0.3-0.5, where the value of 0.5 describes an incompressible material having an elastic deformation at small strains. The rubber's Poisson's ratio (~ 0.49) is applicable for BC.

1.4 Capacitive and piezoresistive responses under loading-unloading cycles

The responses of BC/SPN follow a second-degree polynomial regression. The regression coefficient shows an excellent fit through large coefficient of determinations (R^2 = .9918-.9956). The polynomial equations for BC/SPN were found to be $-4 \cdot 10^{-5}x^2+0.0118x-0.0239$ (capacitive response) and $4 \cdot 10^{-5}x^2-0.0069x-0.0231$ (piezoresistive response) under stretching. The fits imply a strong piezoresistivity and a stress-dependent dielectric behavior. Both capacitive and piezorestive operation modes show negligible hysteresis (< 2%) during stretching-releasing cycles.

1.5 Hooke's law

Hooke's law is applicable for elastomeric materials in a linear stress-strain region. Hooke's law is defined by Equation (S2):

$$\varepsilon = \frac{\sigma}{E} = \frac{F}{AE} \qquad (2)$$

where ε is applied tensile strain, σ is tensile stress, E is Young's modulus, F is applied force and A is the cross-sectional area.

1.6 Response and recovery times under normal pressure

The response and recovery times were measured with Agilent InfiniiVision MSO-X-3054A oscilloscope when using a voltage divider circuit. The voltage over BC/SPN device was measured when connected in series with another resistor. The BC/SPN device showed near instantaneous response (~5 ms) and recovery (~10 ms) to applied pressure of ~50 kPa. The result is similar to that observed with 555-timer circuit when switching intensity of some LEDs (Video S1). Furthermore, we expect that the recovery and response times of the device are nearly identical for piezoresistive and capacitive operation modes as previously shown[S5]. This relates to the uniform structure of the sensor for both operation modes leading to identical deformation under similar stimuli. The voltage divider circuit and oscilloscope eliminate the delay and poor resolution issues of the Labview program that would lead to significantly higher response and recovery times of the BC/SPN device.

1.7 Capacitive responses under normal pressure

Capacitive response under normal pressure can be expresses as Equation (S3):

$$C = (\varepsilon_0 \varepsilon_r A)/d \qquad \text{(S3)}$$

where A is the area of the electrodes and d is the distance between parallel electrodes.

1.8 Comparison of capacitive and piezoresistive operation modes

The piezoresistivity operation mode offers significantly higher normal pressure sensitivity with insensitivity to tensile strain and bending, but it has expected non-linear responses. The advantages of capacitive operation mode are that it mainly relies on dimensional changes offering linearity, higher precision and stability. The absence of transient behavior is another benefit of capacitive sensors. However, the capacitive sensing is negatively affected by environmental noise (when closely fitted) such as natural body capacitance (up to hundreds of pF) and other parasitic sources

(order of tens of pF). This requires high specific capacitances (i.e. capacitance per area) to achieve robustness and immunity from environmental noise.

1.9 Definition for piezoresistivity

The piezoresistivity can be defined as Equation (S4):

$$\frac{\Delta R}{R_0} = (1 + 2v)\varepsilon + \Delta\rho/\rho_0 \qquad \text{(S4)}$$

where v is the Poisson's ratio, Δρ is change of resistivity and ρ_0 is the resistivity when no load is applied to the material.[S4] The piezoresistivity arises from geometrical effects, bulk resistivity change within the material and contact resistance change between active materials and electrodes.

2. Supplementary Figures

Figure S1. Photographs of a sensor.

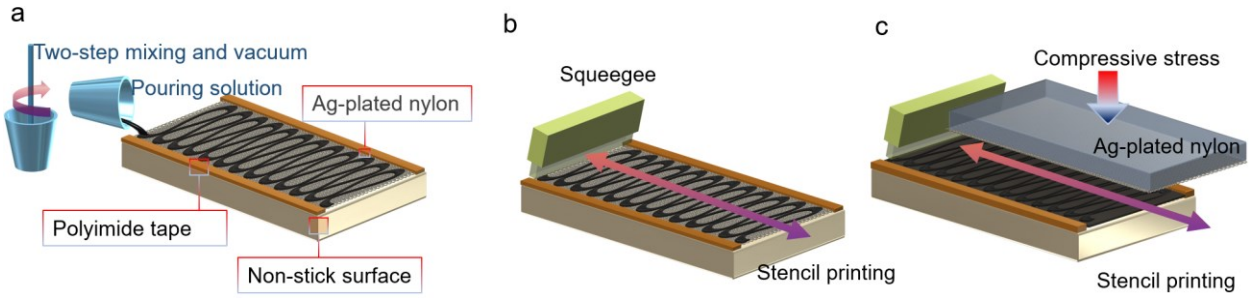

Figure S2. Fabrication process of biocarbon/silver-plated nylon sensor (BC/SPN). (a) Mixing composite solution and pouring onto silver-plated nylon (SPN). (b) Screen-printing composite solution onto SPN. (c) Screen-printing the second composite solution onto composite film layer.

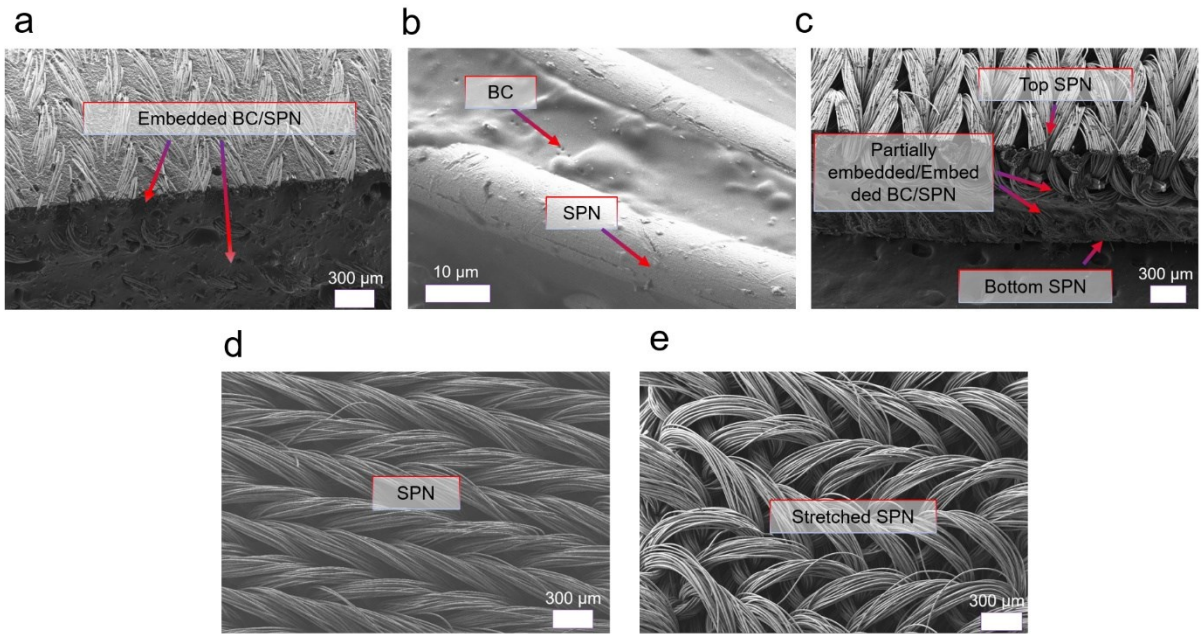

Figure S3. FESEM images of the sensor. (a) Cross-sectional view of the embedded BC/SNP layers. (b) The SPN are covered inside the biocarbon composite. (c) Cross-sectional view of the sensor structure. (d) Surface of SPN when unloaded. (e) Surface of SPN when applying a tensile strain. The porosity increases as the threads of SPN becomes more spacious.

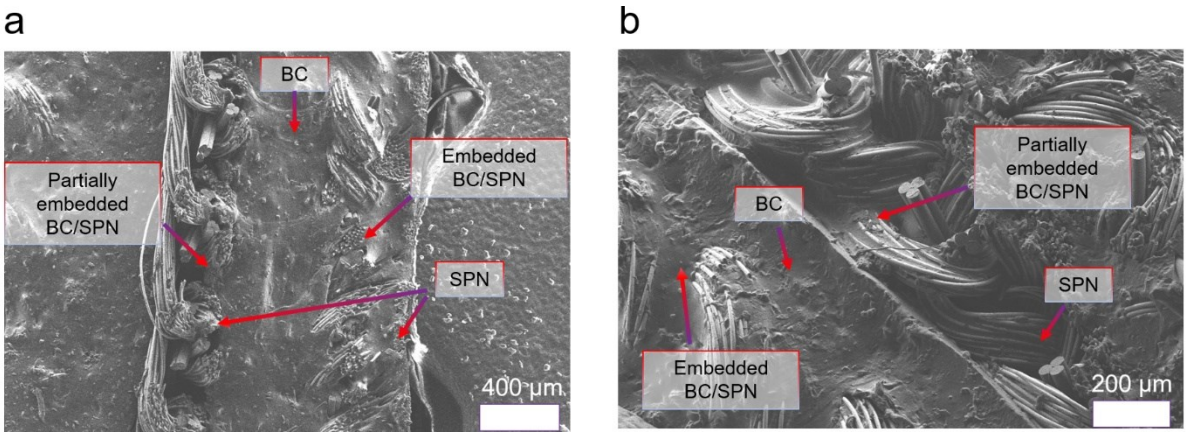

Figure S4. FESEM images of a sensor under compressive stress. (a) Cross-view of the sensor when applying a small normal pressure. (b) Increased normal pressure leads to significant change in the spacing between embedded and partially embedded BC/SPN layers

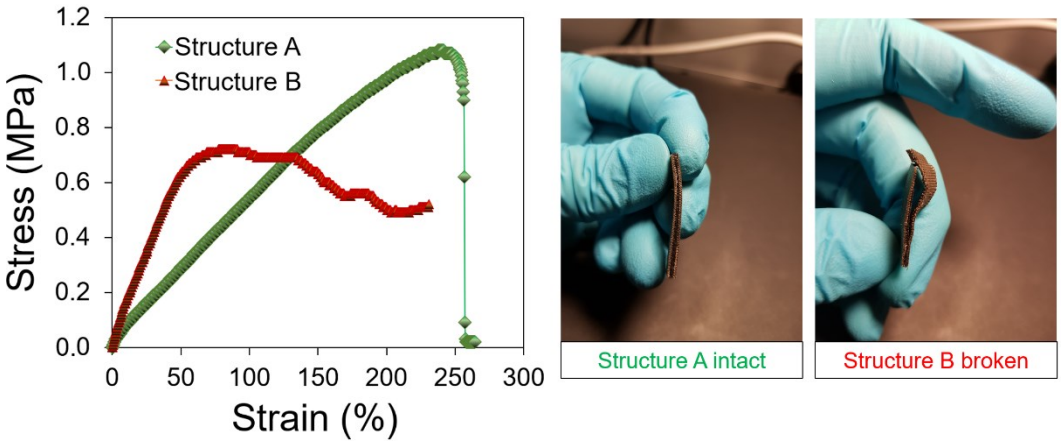

Figure S5. Stress-strain curve for BC/SPN device. The major difference is that structure A has properly embedded BC/SPN interfaces in both printed BC layers. The structure B has poorly embedded interface between SPN and the second printed BC layer.

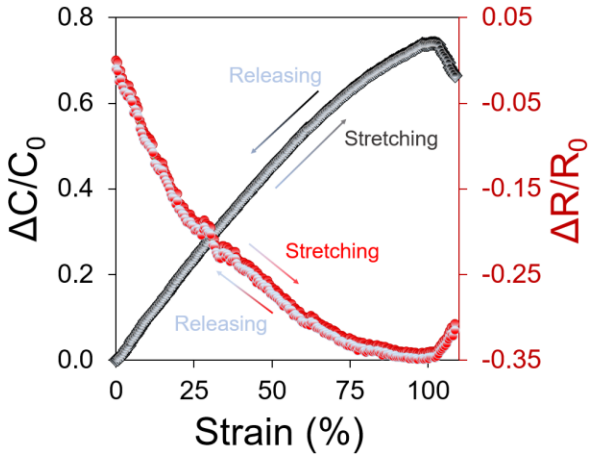

Figure S6. Capacitive and piezoresistive response of BC/SPN sensor under tensile strain. The responses were recorded when applying a tensile strain and then releasing the strain (ε = 0-105% and strain rate ± 2.1% s^{-1}). Measurements were done with amplitude of 1 V, frequency of 1 kHz and in 23 ℃.

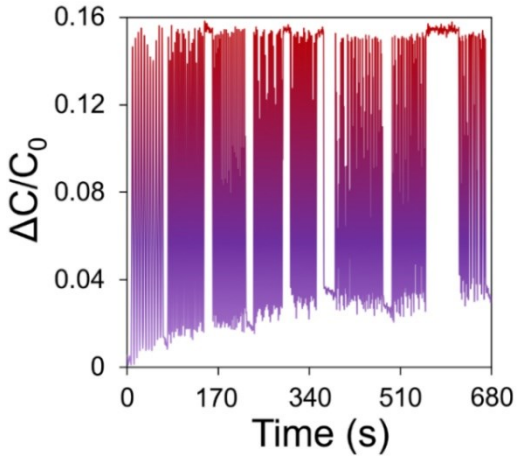

Figure S7. The response of BC/SPN when applying a tensile strain of 25% and increasing strain rate between 10-100% s^{-1}. The variation in $\Delta C/C_0$ when applying strain relates to the measurement accuracy of the Labview program for capacitive measurements.

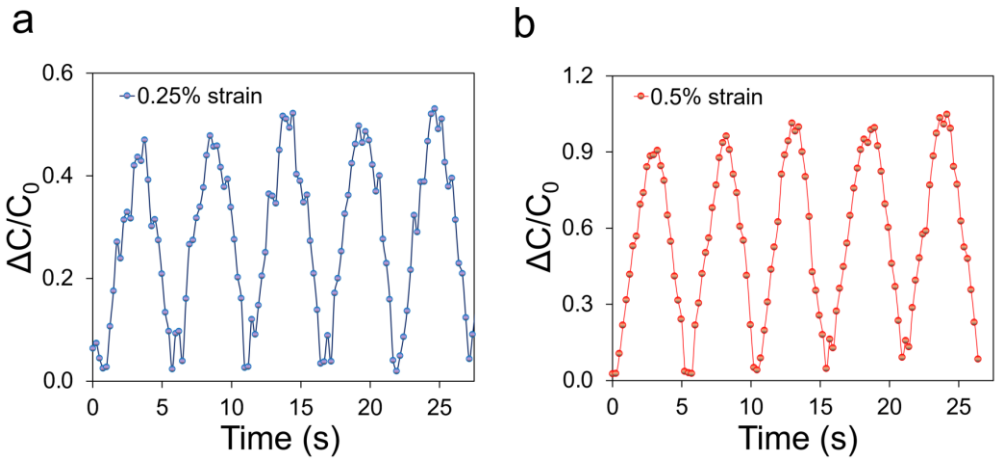

Figure S8. Dynamic responses of BC/SPN to small strain. (a) Tensile strain of 0.25% (strain rate 0.13% s^{-1}) and (b) 0.5% (strain rate 0.50% s^{-1}) were applied. These corresponded to frequency of 0.19 Hz and 0.15 Hz, respectively.

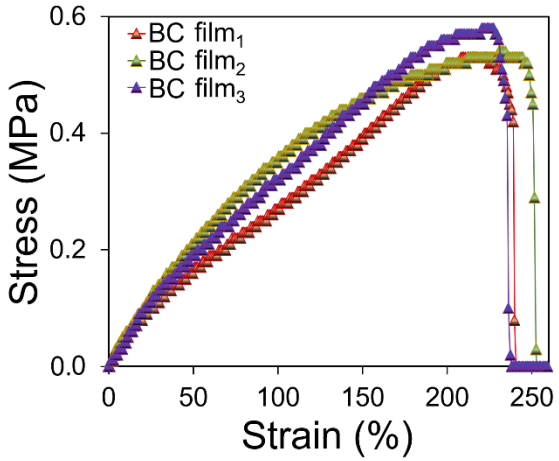

Figure S9. Stress-strain curves for BC films. Films thicknesses were ~300-400 µm. Strain at break for the BC films was observed to be approx. 230%.

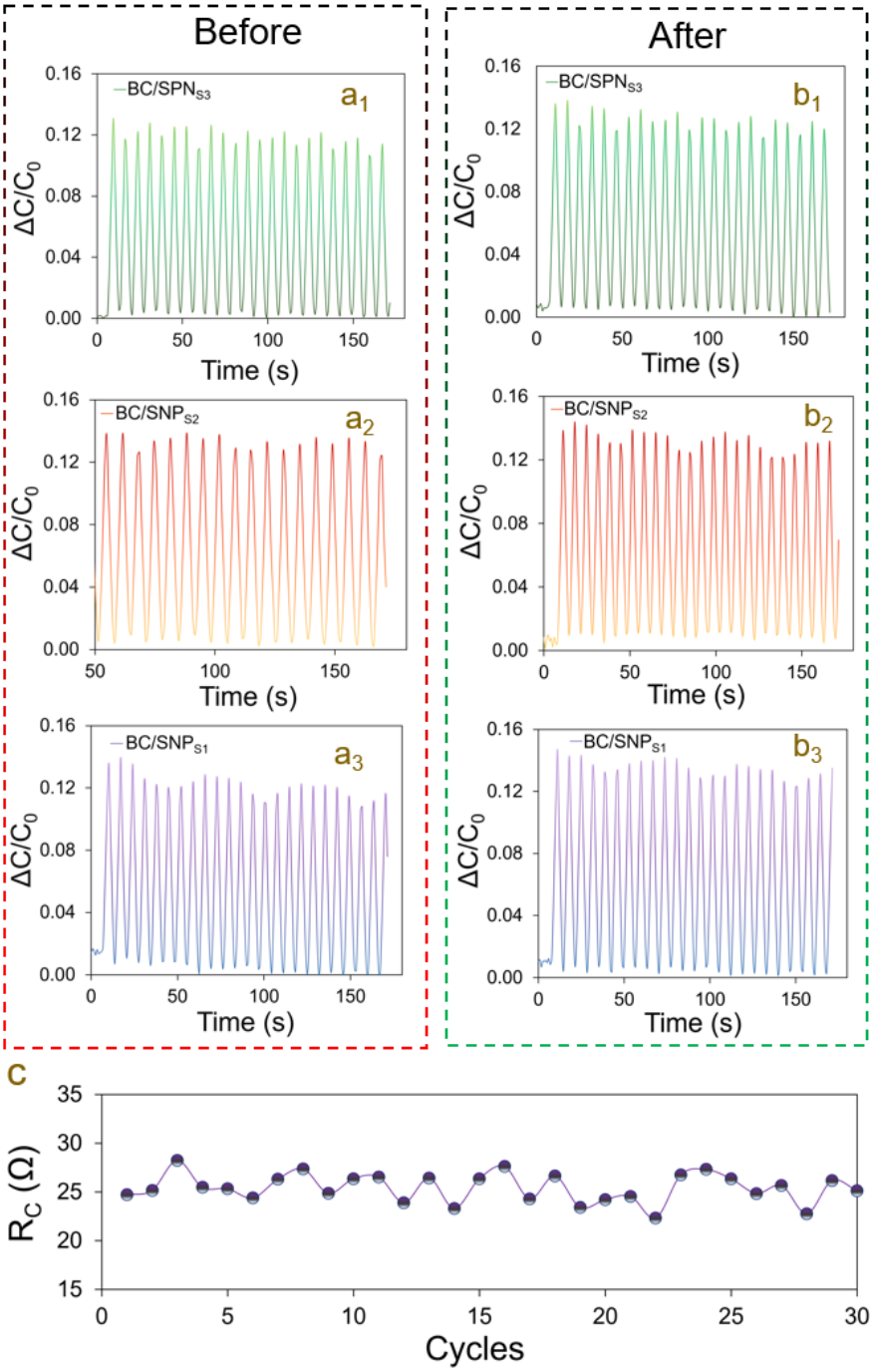

Figure S10. Machine washability testing for BC/SPNs. (a-b) Electromechanical responses of BC/SPNs (strain 20%, strain rate approx. 8% s^{-1}) before machine washing (a_{1-3}) and after 30 cycles (b_{1-3}) in 40 °C and 1200 rpm with drip dried samples. (c) Average contact resistance (direct current) variation during machine washing cycles (> 10 samples) after drip dying samples.

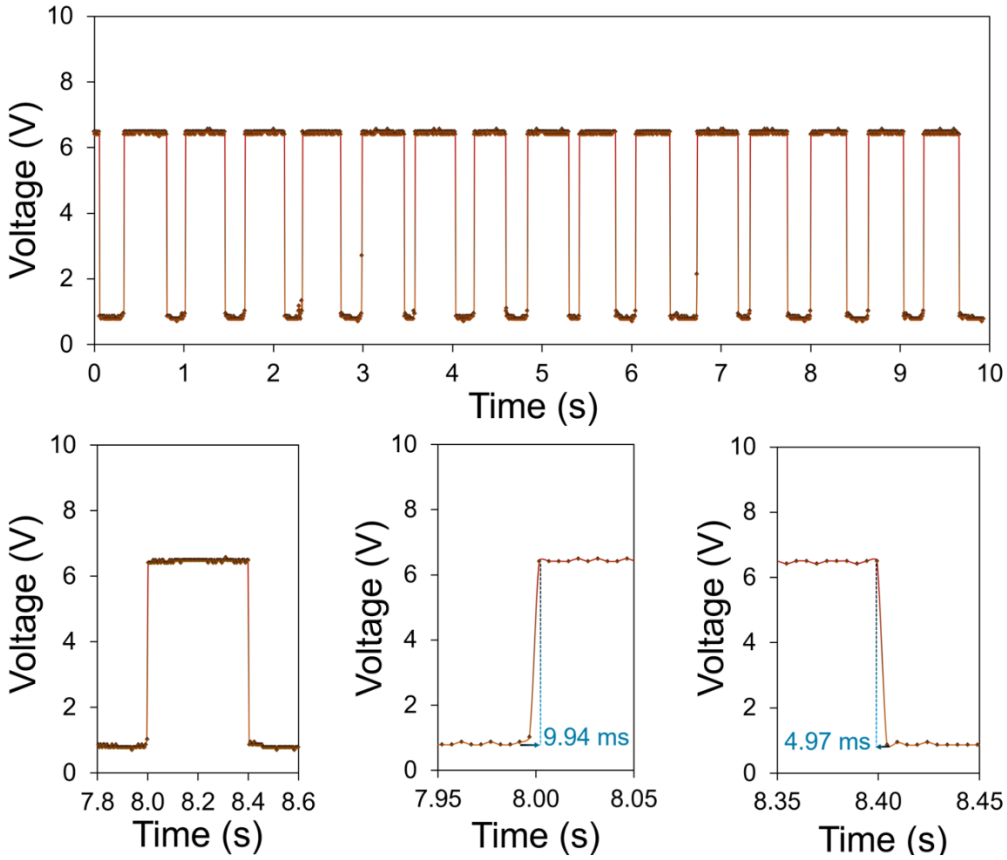

Figure S11. Response and recovery times of a sensor when measured with oscilloscope and voltage divider circuit when applying normal pressure of ~50 kPa.

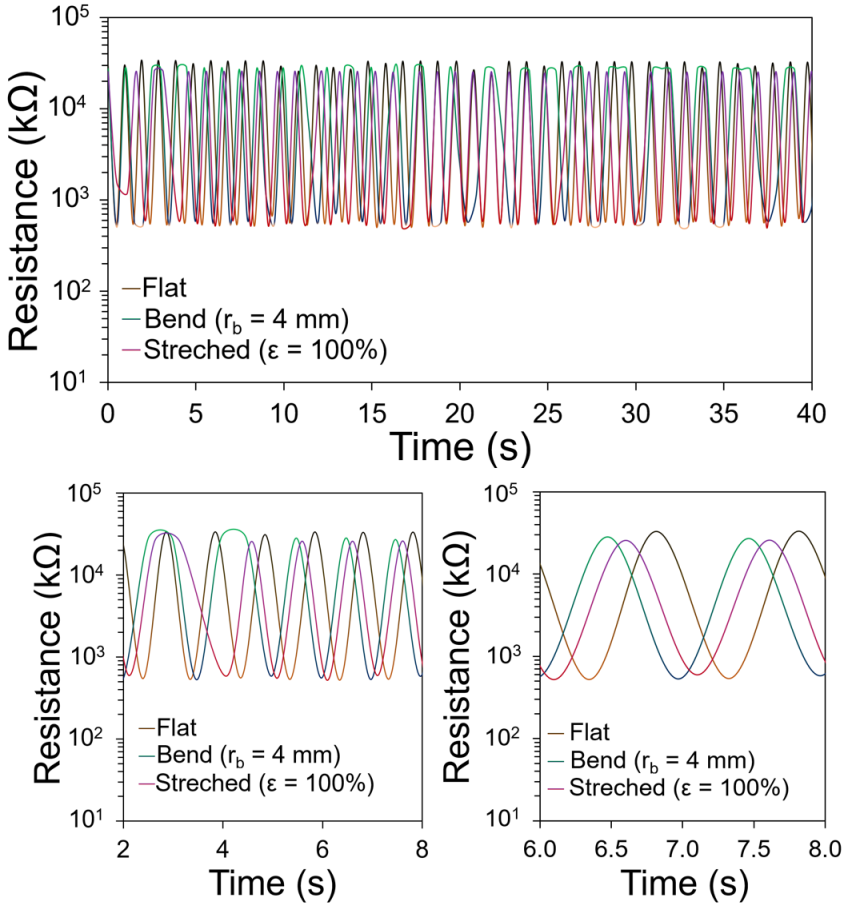

Figure S12. Piezoresistive responses of a sensor to applied normal pressure of ~25 kPa. Flat, bended (r_b = 4 mm) and stretched (ε = 100%) states are compared to each other.

3. Supplementary Tables

Table S1. Summary of bending-insensitive sensors.

Working principle	Materials	Maximum sensitivity (kPa^{-1})	Range (kPa)	Response times (ms)	Thickness (μm)	Bending sensitivity (% mm^{-1})	Min. bending radius (mm)	Stretchability (%)	Reference
Capacitive	NPB/AgNP	0.036	< 3	50	45	-	-	-	[S6]
Resistive/ Capacitive	ITO/PET/ PDMS	44.5 / 449	< 0.1 / 0.01	50-100 / 9-30	-	~0.15	5.0	50	[S7]
Resistive	CNT/PDMS	0.01	1200	8-10	< 3000	~0.67	7.5	-	[S8]
Resistive	FCP/CNT/ graphene	> 10^6	~1	5-20	2	~0.00	0.08	-	[S9]
Resistive	BC/SPN	60.8	50	5-10	~1100	~0.36	< 4.0	> 200	This work

Table S2. Properties of the device under two different operation modes.

Operation Mode	Strain Sensitivity (GF)	Bending Sensitivity (% mm^{-1})	Pressure Sensitivity (kPa^{-1})	Linearity[a)]	Degree of Hysteresis[b)]	Response/Recovery times (ms)
Piezoresistive	-0.35	-0.358	60	No	< 2%	< 10
Capacitive	0.75	1.334	0.005	Yes	< 2%	(expected to be identical)

[a)]The capacitive operation mode shows relative linear behavior when sensing tensile strain (< 100%) and normal pressure (coefficient of determination (R^2) > .95); [b)] Maximum hysteresis values when applying tensile strain up to 100%. Degree of hysteresis with strain rates of 2.1% s^{-1} were calculated as $(\frac{(|H_{U\varepsilon}|-|H_{L\varepsilon}|)}{|H_{L\varepsilon}|}\cdot 100\%$, where $H_{U\varepsilon}$ is value of resistance/capacitance at specific load when decreasing the tensile strain and $H_{L\varepsilon}$ is value of resistance/capacitance at specific load when increasing the tensile strain.

Table S3. Average electrical properties for pyrolyzed pine and pyrolyzed pine/urethane rubber composite films with 5 wt.% filler loading (~10 samples).

Material	Resistance (MΩ)	Resistivity (Ω·m)	Conductivity (10^{-7} S/m)
Pyrolized pine	~264	~660	~15100
Biocarbon composite (5 wt %)	~63600	~5089000	~2

Table S4. Summary of resistive and capacitive switching devices that are based on applied stretching or external pressure.

Working principle	Materials	On/off ratio	Response /recovery time (ms)	Stretchability (%)	Tunable switching range	Durability/ Stability	Reference
Resistive	SWCNT/PDMS	~10^6 (50 kPa)	- / 7 (200 kPa)	100	~10-700 kPa	> 300 cycles	[S10]
Resistive	Polypyrrole	~10^3 (2 kPa)	50 / -	No	No	-	[S11]
Resistive	AgNW/PDMS/cloth	~10^7 (1 kPa)	4 / 16	-	No	> 5k cycles	[S12]
Capacitive	PDPP3T	~10^3 (4 kPa)	< 10 / -	No	No	>100k cycles (1 kPa)	[S13]
Resisitive	G-PDMS/RGO	~10^5 (350%)	145 / -	350	No	> 5k cycles (50%)	[S14]
Resistive	E-GWF/PDMS	~10^5 (50%)	70 / -	~50	No	> 5k cycles (50%)	[S15]
Resistive	Ag-DS/CF[a)]	~10^5 (70%)	20 / -	75	~5-75%	>3k cycles (20%)	[S16]
Resistive	Ag/laser-cut film	10^{12} (0.006%)	-	< 30	No	15M cycles (0.4%)	[S17]
Resistive	BC/SPN[b)]	~10^3 (50 kPa)	5 / 10 (~50 kPa)	> 200	~20-500 kPa	> 10k cycles (20% and 90°)	This work

[a)] Machine washable for 3 cycles (40 °C, 1200 rpm, 30 min/cycle); [b)] Machine washable for 30 cycles (40 °C, 1200 rpm, ~45 min/cycle, mesh bag)

4. Supplementary References

(1) Huang, M.; Tunnicliffe, L. B.; Zhuang, J.; Ren, W.; Yan, H.; Busfield, J. J. C. Strain-Dependent Dielectric Behavior of Carbon Black Reinforced Natural Rubber. *Macromolecules* **2016**. https://doi.org/10.1021/acs.macromol.5b02332.

(2) Atalay, A.; Sanchez, V.; Atalay, O.; Vogt, D. M.; Haufe, F.; Wood, R. J.; Walsh, C. J. Batch Fabrication of Customizable Silicone-Textile Composite Capacitive Strain Sensors for Human Motion Tracking. *Adv. Mater. Technol.* **2017**, *2* (9). https://doi.org/10.1002/admt.201700136.

(3) Tolvanen, J.; Hannu, J.; Nelo, M.; Juuti, J.; Jantunen, H. Dielectric Properties of Novel Polyurethane-PZT-Graphite Foam Composites. *Smart Mater. Struct.* **2016**, *25* (9). https://doi.org/10.1088/0964-1726/25/9/095039.

(4) Shi, G.; Zhao, Z.; Pai, J. H.; Lee, I.; Zhang, L.; Stevenson, C.; Ishara, K.; Zhang, R.; Zhu, H.; Ma, J. Highly Sensitive, Wearable, Durable Strain Sensors and Stretchable Conductors Using Graphene/Silicon Rubber Composites. *Adv. Funct. Mater.* **2016**, *26* (42), 7614–7625. https://doi.org/10.1002/adfm.201602619.

(5) Tolvanen, J., Hannu, J., Jantunen, H. Hybrid Foam Pressure Sensor Utilizing Piezoresistive and Capacitive Senging Mechanisms. IEEE Sensors Journal **2017**, 17(15), 4735-4746. https://doi.org/10.1109/JSEN.2017.2718045

(6) Yoo, J-Y., Seo, M-H.; Lee, J-S.; Choi, K-W.; Jo, M-S.; Yoon, J-B. Industrial Grade, Bending-Insensitive, Transparent Nanoforce Touch Sensor via Enhanced Percolation Effect in a Hierarchical Nanocomposite Film, Adv. Func. Mater. **2018**, 28, 1804721. https://doi.org/10.1002/adfm.201804721

(7) Yang, J. C.; Kim, J-O.; Oh, J.; Kwon, S. Y.; Sim, J. Y.; Kim, D. W.; Choi, H. B.; Park, S. Microstructure Porous Pyramid-Based Ultrahigh Sensitive Pressure Sensor Insensitive to Strain and Temperature. ACS Appl. Mater. Interfaces, **2019**, 11, 19472-19480. https://doi.org/10.1021/acsami.9b03261

(8) Kim, S.; Amjadi, M.; Lee, T. I:; Jeong, Y.; Kwon, D.; Kim, M. S.; Kim, K.; Kim, T.S.; Oh, Y. S.; Park., I. Wearable, Ultrawide-Range, and Bending-Insensitive Pressure Sensors Based on Carbon Nanotube Network-Coated Porous Elastomer Sponges for Human Interface and Healthcare Devices. ACS Appl. Mater. Interfaces, 2019, 11, 23639-23648. https://doi.org/10.1021/acsami.9b07636

(9) Lee, S.; Reuveny, A.; Reeder, J.; Lee, S.; Jin, H.; Liu, Q.; Yokota, T.; Sekitani, T.; Isoyama, T.; Abe, Y.; Suo, Z.; Someya, T. A transparent bending-insentive pressure sensor. Nature Nanotechnology, 2016, 11, 472-478. https://doi.org/10.1038/nnano.2015.324

(10) Chou, H. H.; Nguyen, A.; Chortos, A.; To, J. W. F.; Lu, C.; Mei, J.; Kurosawa, T.; Bae, W. G.; Tok, J. B. H.; Bao, Z. A Chameleon-Inspired Stretchable Electronic Skin with Interactive Colour Changing Controlled by Tactile Sensing. *Nat. Commun.* **2015**, *6*, 1–10. https://doi.org/10.1038/ncomms9011.

(11) Pan, L.; Chortos, A.; Yu, G.; Wang, Y.; Isaacson, S.; Allen, R.; Shi, Y.; Dauskardt, R.; Bao, Z. An Ultra-Sensitive Resistive Pressure Sensor Based on Hollow-Sphere Microstructure Induced Elasticity in Conducting Polymer Film. *Nat. Commun.* **2014**. https://doi.org/10.1038/ncomms4002.

(12) Lai, Y. C.; Ye, B. W.; Lu, C. F.; Chen, C. T.; Jao, M. H.; Su, W. F.; Hung, W. Y.; Lin, T. Y.; Chen, Y. F. Extraordinarily Sensitive and Low-Voltage Operational Cloth-Based Electronic Skin for Wearable Sensing and Multifunctional Integration Uses: A Tactile-Induced Insulating-to-Conducting Transition. *Adv. Funct. Mater.* **2016**, *26* (8), 1286–1295. https://doi.org/10.1002/adfm.201503606.

(13) Zang, Y.; Zhang, F.; Huang, D.; Gao, X.; Di, C. A.; Zhu, D. Flexible Suspended Gate Organic Thin-Film Transistors for Ultra-Sensitive Pressure Detection. *Nat. Commun.* **2015**. https://doi.org/10.1038/ncomms7269.

(14) Ma, J.; Wang, P.; Chen, H.; Bao, S.; Chen, W.; Lu, H. Highly Sensitive and Large-Range Strain Sensor with a Self- Compensated Two-Order Structure for Human Motion Detection. *ACS Appl. Mater. Interfaces* **2019**, *11*, 8527–8536. https://doi.org/10.1021/acsami.8b20902.

(15) Liu, X.; Liu, D.; Lee, J. H.; Zheng, Q.; Du, X.; Zhang, X.; Xu, H.; Wang, Z.; Wu, Y.; Shen, X.; Cui, J.; Mai, Y-W.; Kim, J-K. Spider-Web-Inspired Stretchable Graphene Woven Fabric for Highly Sensitive, Transparent, Wearable Strain Sensors. *ACS Appl. Mater. Interfaces* **2018**, *11*, 2282–2294. https://doi.org/10.1021/acsami.8b18312.

(16) Tolvanen, J.; Hannu, J.; Jantunen, H. Stretchable and Washable Strain Sensor Based on Cracking Structure for Human Motion Monitoring. *Sci. Rep.* **2018**, No. August, 1–10. https://doi.org/10.1038/s41598-018-31628-7.

(17) Tolvanen, J.; Hannu, J.; Palosaari, J.; Nelo, M.; Jantunen, H. Screen-Printed Mechanical Switch Based on Stretchable PU-Foam Film. *Electron. Lett.* **2016**, *52* (16). https://doi.org/10.1049/el.2016.2002.